Developmental Cell, Volume *47*

Supplemental Information

ARP3 Controls the Podocyte Architecture at the Kidney Filtration Barrier

Christoph Schell, Benedikt Sabass, Martin Helmstaedter, Felix Geist, Ahmed Abed, Mako Yasuda-Yamahara, August Sigle, Jasmin I. Maier, Florian Grahammer, Florian Siegerist, Nadine Artelt, Nicole Endlich, Dontscho Kerjaschki, Hans-Henning Arnold, Jörn Dengjel, Manuel Rogg, and Tobias B. Huber

Supplementary Figure Legends

Figure S1. Podocyte proteomic analysis, Related Figure 1
(a) Complete mapped proteome from Figure 1. Network analysis of *in vivo* podocyte enriched cytoskeletal proteins revealed distinct functional subsets such as actin binding or focal adhesion associated proteins as indicated (see also Figure 1 and Table S1). Filtering of the list revealed a subset of proteins centrally involved in the aforementioned processes (highlighted yellow). **(b)** Venn diagram comparing the coverage of functional clustered proteins in the in-vivo podocyte proteome (see also Figure 1 and Table S1). **(c)** Venn diagram comparing the coverage of detected proteins between a recently published proteomics based meta-adhesome[41], the GO-Term "focal adhesion" and the actual MS based screening approach for podocyte focal adhesion proteins. **(d)** Comparison of the coverage of intensity/enrichment grouped proteins between the meta-adhesome and the actual podocyte adhesome screening approach revealed a strong correlation between intensity group and coverage with the meta-adhesome and thereby indirectly validated the current dataset (rank 0-5% means the protein MS intensity is greater than the MS intensity of 95% of adhesome detected proteins). **(e)** Mapping of the recently described consensus integrin adhesome[41], the Arp2/3 complex and the Myosin II complex. The enrichment of mapped proteins in the podocyte adhesome screening approach is highlighted as indicated (for detailed information see Table S2).

Figure S2. Expression and localization of N-WASP and ARP3, Related to Figure 1
(a-b) Immunofluorescence studies of N-WASP and ARP3 localization in human glomeruli (a-b; overview images as in main figure 1, dotted lines indicate glomeruli). **(c)** Immunofluorescence microscopy demonstrating co-localization of ARP3 and PAXILLIN during early phases of cellular spreading in wild type primary podocytes (white box indicates area of higher magnification; overview image as in main figure 1). **(d)** Western blot of total cell lysates and focal adhesion fraction demonstrating an increase of bona-fide FA proteins (ITGB1 – integrin beta1, ACTN4 – actinin-4) in the FA fraction. **(e&f)** Immunofluorescence studies on adult mouse glomeruli demonstrated predominant localization of ARP3 and N-WASP at the basal compartment of podocytes (NPHS1 – Nephrin was used to visualize the podocyte compartment). **(g&h)** Co-staining of N-WASP with LTG (lotus tetragonolobus lectin) as a marker for proximal tubules showed no detectable expression of N-WASP in proximal tubules of adult mice kidneys. **(i-m)** Co-staining of N-WASP with LTG, DBA and THP revealed expression of N-WASP within distal segments of the nephron; major co-localization with DBA and partially with THP (LTG – marker for the proximal tubule compartment, lotus tetragonolubus; DBA – marker for collecting duct system, dolichos biflorus agglutinin; THP – marker for loop of henle, tamm horsefall protein).

Figure S3. Knockout of *N-WASP* in murine podocytes and tubular compartments, Related to Figure 2
(a) Schematic illustrating the strategy for different *Cre* lines to generate viable and podocyte specific knockouts for *N-WASP* and *Arp3*. **(b&c)** Analysis of body weight gain and correlating kidney weight indicated pronounced hypomorphic growth of *N-WASP* KO mice (at least 4 animals at each time point were analyzed, ** $p<0.01$, *** $p<0.001$, **** $p<0.0001$) **(d&e)** Additional data for Figure 2 f-g, overviews and crops: immunofluorescence staining for NEPHRIN and WT1 demonstrated dilated capillary formation in *N-WASP**Six2Cre knockout animals (white arrows indicate defective in-folding; dotted lines mark glomerular outlines). **(h&i)** Histology of p3 *N-WASP*Six2Cre* kidney sections shows present proximal tubules. Given the proteinuric phenotype of respective knockout animals protein droplets can be detected (white asterisk). **(j-n)** Deletion of N-WASP employing the inducible *Pax8*tetO-cre* system (leading to inducible *Cre* recombination and deletion in the whole tubular compartment upon application of doxycycline) at different time points did not lead to any overt phenotype in terms of decreased body weight. Histologic analysis does not indicate major structural abnormalities in respective *N-WASP*Pax8-rtTA*teto-cre* knockout animals

(n=8 WT and 5 KO mice were analyzed after embryonic induction; n= 8 WT and 8 KO mice were analyzed after adult induction; n.s. – non significant).

Figure S4. Analysis of *Arp3* knockout kidneys and primary podocytes, Related to Figure 2 and 3

(a&b) Histological evaluation revealed increasing signs of glomerular damage in respective *Arp3* KO animals (yellow asterisks indicate areas of sclerosis, black arrows indicate proteinaceous casts). **(c)** Quantification of glomerular damage showed first significant changes already at p7 between wild type and respective *Arp3* KO animals (categories of glomerular damage according to standardized sclerosis score: 0 - no changes, I - mild mesangial expansion, sclerosis <25%, II - meangial expansion, sclerosis >25, <75%, III - >75% sclerosis; 3 animals for each genotype were analyzed. (N.S. – non significant; * p<0.05, ** p<0.01, *** p<0.001, **** p<0.0001)). **(d)** At p14 typical slit diaphragm markers like NEPHRIN and PODOCIN showed an almost unaffected distribution and signal intensity in *Arp3* KO animals. **(e)** The podocyte cytoskeleton associated protein SYNAPTOPODIN was also observed in normal distribution and intensity (note that ARP3 signal is still present in the mesangial compartment, whereas no signal is detectable in the podocyte compartment - dotted lines). **(g-i)** Transmission electron microscopy of *Arp3* KO mice detected misconfigured podocyte foot processes and disrupted localization of slit diaphragms (yellow arrows). **(j-l)** Overview of 3D-SIM microscopy in respective wild type animals; single plane zoom-ins illustrate FP architecture. **(m)** Representative single plane images of maximum intensity projections from 3D cultured primary *Arp3* WT and KO podocytes in main Figure 3f and 3g. **(n)** Visualization of filamentous actin by Phalloidin staining highlighted the absence of lamellipodial structures in respective knockout podocytes. In arc-like regions between cellular protrusions, actin networks accumulated to mesh-work structures in *Arp3* KO cells (highlighted by red colored dotted box). **(o)** Quantification of filopodia per cell revealed a pronounced increase of these structures in ARP3 deleted podocytes (38 wild type and 41 *Arp3* KO cells were analyzed, **** p<0.0001). **(p)** Stress fiber numbers per cell were unaffected by deletion of ARP3 (38 wild type and 41 ARP3 KO cells were analyzed, n.s. – non significant). **(r-t)** Immunofluorescence staining for PAXILLIN, VINCULIN and ZYXIN in *Arp3* wild type and knockout cells demonstrated accumulation of ZYXIN in FA plaques of *Arp3* knockout cells (white lines indicate cellular outlines; dotted boxes mark regions of higher magnification; yellow lines indicate areas used for line scan analysis; RFU – relative fluorescence unit; a.u. - arbitrary unit).

Figure S5. Functional analysis of primary *N-WASP* and *Arp3* podocytes, Related to Figure 4 and 5

(a) Altered focal adhesion (FA) morphology of *Arp3* KO podocytes was independent of ECM composition, as either coating by fibronectin or collagen IV resulted in increased adhesion sites in *Arp3* KO primary podocytes (16 wild type and 17 *Arp3* KO cells were analyzed; ** p<0.01, *** p<0.001). **(b)** Overview images of Figure 4-f: Immunofluorescence staining for PAXILLIN and F-ACTIN (Phalloidin) demonstrates normal lamellipodium and focal adhesion structures in *N-WASP* knockout podocytes. **(c)** Cortactin immunofluorescence staining in *N-WASP* KO primary podocytes reveals a distinct localization at the lamellipodial edge and confirmed lamellipodia formation in *N-WASP* KO podocytes. **(d-f)** The Arp2/3 complex activating NPF (actin nucleation promoting factor) WAVE2 is expressed in primary WT and *N-WASP* KO podocytes and localize to lamellipodia in 2D. Inhibition of the WAVE2 upstream activator RAC1 by NSC-23766 disrupted lamellipodia formation and WAVE2 localization in primary podocytes. WAVE2 was visualized by immunofluorescence staining. **(g-i)** Inhibition of the RAC1-WAVE2 axis by NSC-23766 resulted in increased average focal adhesion (FA) size and FA plaque formation in *N-WASP* KO podocytes. FAs were stained by PAXILLIN (average FA size of n=17 DMSO treated and 16 NSC-23766 treated primary *N-WASP* KO podocytes was analyzed; ** p<0.01). **(j-m)** Additional data and overview pictures for Figure 4: Immunofluorescence for NMHC-IIA and ACTN4 demonstrated a sarcomere-like localization pattern on ventral stress fibers in respective *Arp3* knockout cells (dashed yellow lines

indicate regions for line scan analysis; FA – focal adhesion; SF – stress fiber). **(n&o)** Immunofluorescence staining for pp-MLC in wild type and ARP3 knockout glomeruli; higher magnifications are pseudo-colored to visualize levels of intensity (a-2 and b-2, respectively). **(p)** Additional 3D cell reconstructions for Figure 5a-c: Blebbistatin treatment of *Arp3* KO primary podocytes resulted in the formation of simplified protrusions. **(q)** Inhibition of formin based actin nucleation in immortalized human podocytes by different concentrations of SMIFH2. SMIFH2 treatment reduced podocyte process formation on collagen gels in a dose dependent manner, as shown by increased circularity scores (n=32 DMSO, 40 5µM SMIFH2 and 42 15µM SMIFH2 treated cells were analyzed; n.s. – non significant, ** p<0.01). **(r-s)** Exemplary z-stack maximum intensity projections of control, CK666 and CK666+blebbistatin treated primary podocytes in 3D culture conditions. Treatment with the Arp2/3 complex inhibitors CK584 or CK666 resulted in increased circularity scores, reflecting simplified cellular morphology in 3D culture. The effect of CK666 could be partially reversed using the myosin inhibitor blebbistatin (38 DMSO, 30 CK548, 87 CK666 and 73 CK666+blebbistatin treated cells were analyzed; **** p <0.0001). **(t)** Freshly isolated kidneys of adult mice were dissected into thin slices and cultured in RPMI medium for 3 hours at 37°C. Slice cultures were treated with DMSO or the Arp2/3 inhibitor CK869 for 3 hours. SEM analysis of treated kidney slices revealed increased levels of dis-organization and morphological alterations by Arp2/3 inhibition.

Figure S6. Role of *Arp3* for podocyte maintenance and mechano-adaptive plasticity, Related to Figure 6

(a) Pre-treatment of *Arp3* knockout cells with blebbistatin reversed the *Arp3* knockout dependent migratory deficit compared to wild type control cells (at least 20 cells per condition were analyzed; n.s. – non significant; **** p<0,0001). **(b-d)** Inhibition of Arp2/3 nucleation by CK666 alters focal adhesion morphology and results in a phenocopy of *Arp3* knockout cells (n=13 ctrl. and 18 CK666 treated cells; ** p<0.01). **(e)** Treatment of immortalized podocytes with different Arp2/3 inhibitors in comparison to modulators of actin polymerization (SMIFH2, LatA, CytoD) or actomyosin activity (Y-27632, blebbistatin) with a focus on focal adhesion (FA) types and morphology. **(f-j)** Treatment of primary podocytes with blebbistatin or Calyculin-A resulted either in dissolution of mature FAs (i&j), or increase in FA area respectively (at least 22 cells per condition were analyzed; * p<0.05, ** p<0.01, *** p<0.001, **** p<0.0001). **(k-l)** Additional data for Figure 6 a-f: Quantification of parameters such as polarization and stress fibers under stressed conditions revealed an adaptive deficit in *Arp3* knockout cells when compared to wild type controls (at least 50 cells per condition were analyzed; n.s. – non significant; ** p<0.01, **** p<0,0001). **(m)** Additional data for Figure 6p. DAPI staining for nuclei. **(n&o)** Overview of 3D-SIM microscopy in respective wild type and inducible *Arp3* KO animals; zoom-ins illustrate misconfigured filtration barrier morphology indicative of aberrant FP architecture in inducible KO mice.

Figure S7 Graphical summary and uncropped western blots, Related to Figure 7

(a&b) Graphical summary.

Figure S1

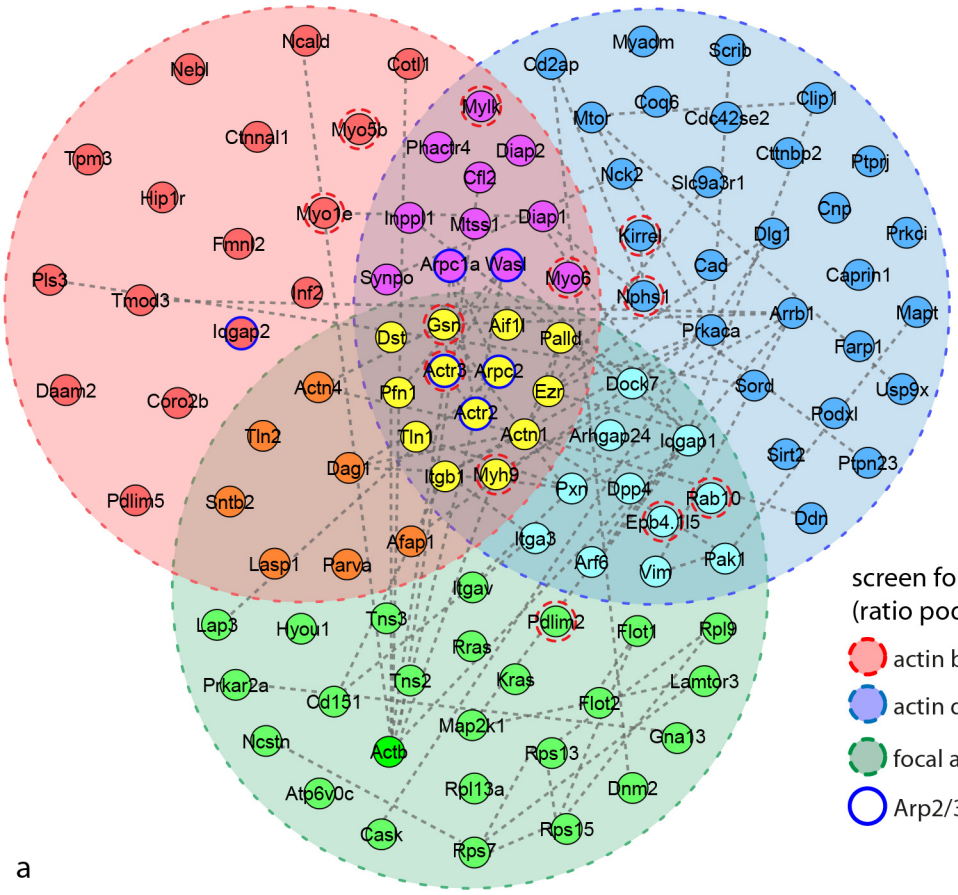

a

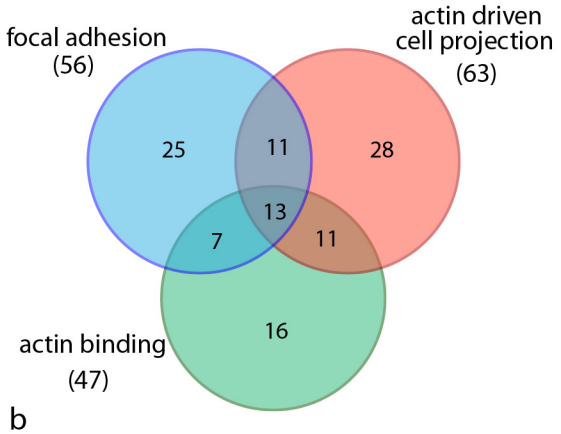

b

screen for podocyte enriched proteins
(ratio podocyte/non-podocyte > 2)

- actin binding
- actin driven cell projection
- focal adhesion
- Arp2/3 associated protein
- Myosin associated protein
- top 10% fraction in podocyte FAP screen

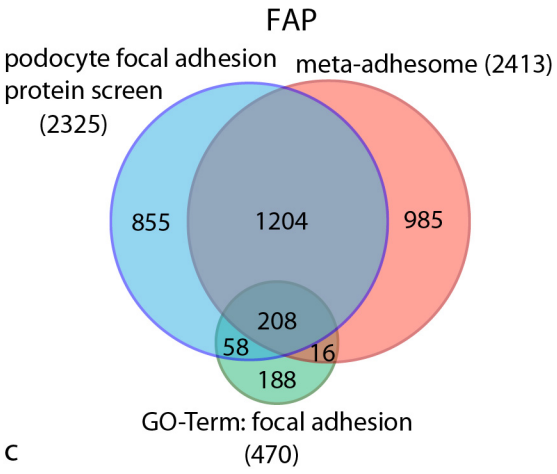

c

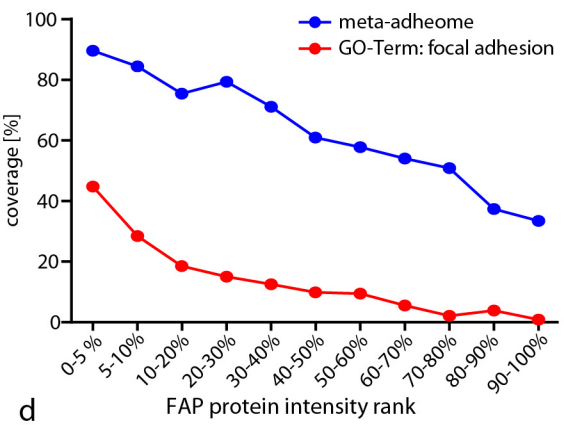

d

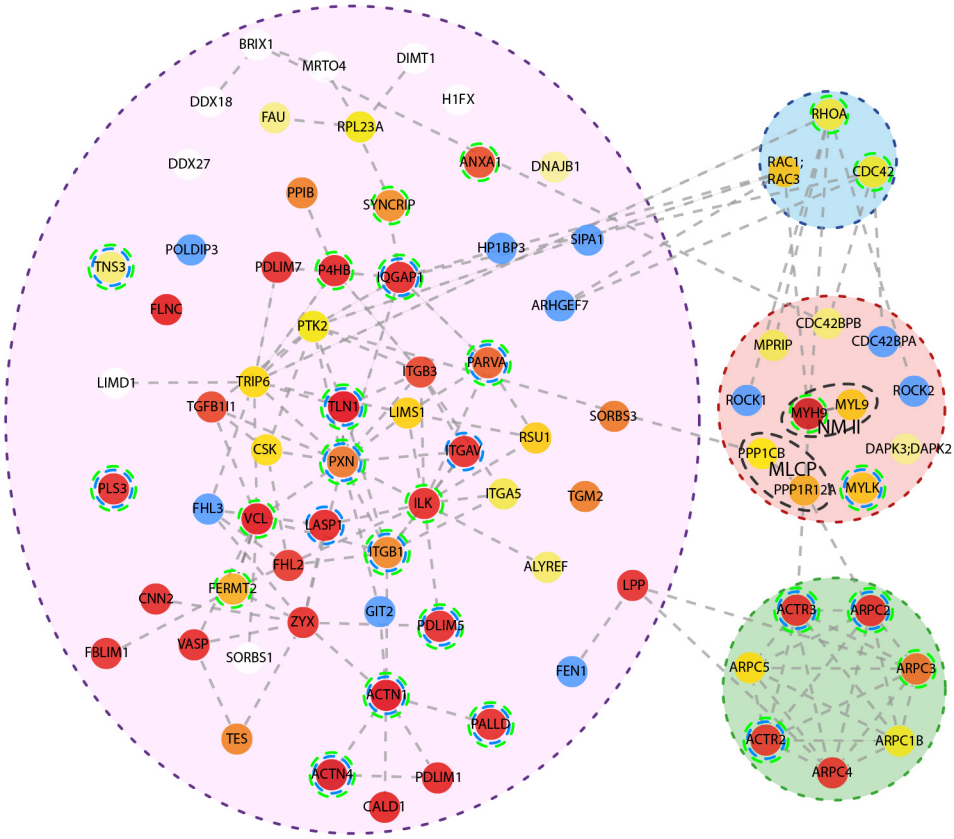

e

human podocyte
focal adhesion protein screen

- consensus integrin adhesome
- small GTPase
- Myosin II - regulation
- Arp2/3 - complex
- not detected in FAP
- < top 50% fraction in FAP
- ratio podocyte/non-podocyte > 2 in podocyte fingerprint
- top 10% fraction in podocyte fingerprint

50% 30% 10% 5% 1%

FAP protein intensity rank

Figure S2

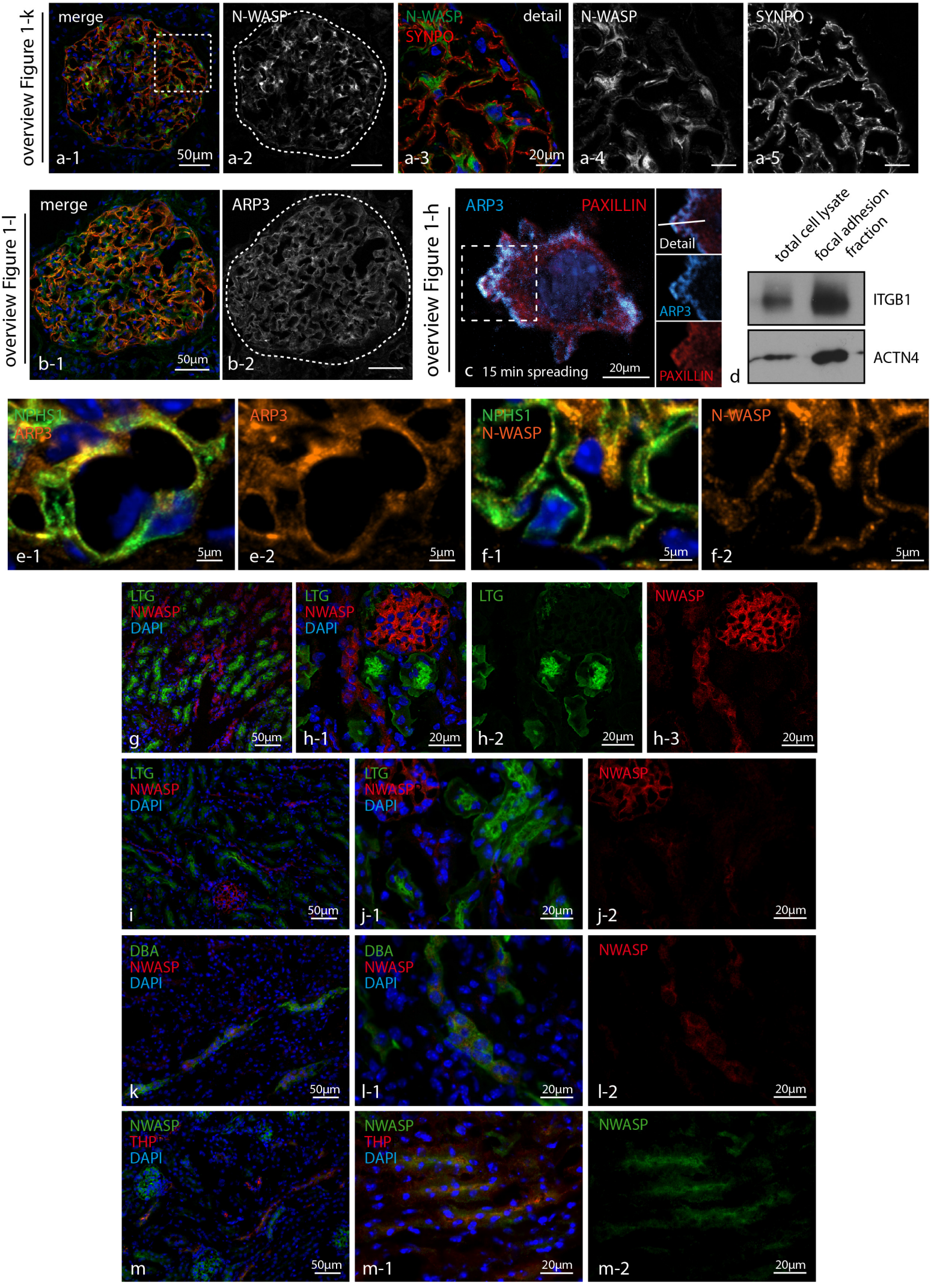
overview Figure 1-k
merge
a-1
50µm
N-WASP
a-2
N-WASP
SYNPO
detail
a-3
20µm
N-WASP
a-4
SYNPO
a-5
overview Figure 1-l
merge
b-1
50µm
ARP3
b-2
overview Figure 1-h
ARP3
PAXILLIN
c 15 min spreading
20µm
Detail
ARP3
PAXILLIN
total cell lysate
focal adhesion fraction
ITGB1
ACTN4
d
NPHS1
ARP3
e-1
5µm
ARP3
e-2
5µm
NPHS1
N-WASP
f-1
5µm
N-WASP
f-2
5µm
LTG
NWASP
DAPI
g
50µm
LTG
NWASP
DAPI
h-1
20µm
LTG
h-2
20µm
NWASP
h-3
20µm
LTG
NWASP
DAPI
i
50µm
LTG
NWASP
DAPI
j-1
20µm
NWASP
j-2
20µm
DBA
NWASP
DAPI
k
50µm
DBA
NWASP
DAPI
l-1
20µm
NWASP
l-2
20µm
NWASP
THP
DAPI
m
50µm
NWASP
THP
DAPI
m-1
20µm
NWASP
m-2
20µm

Figure S3

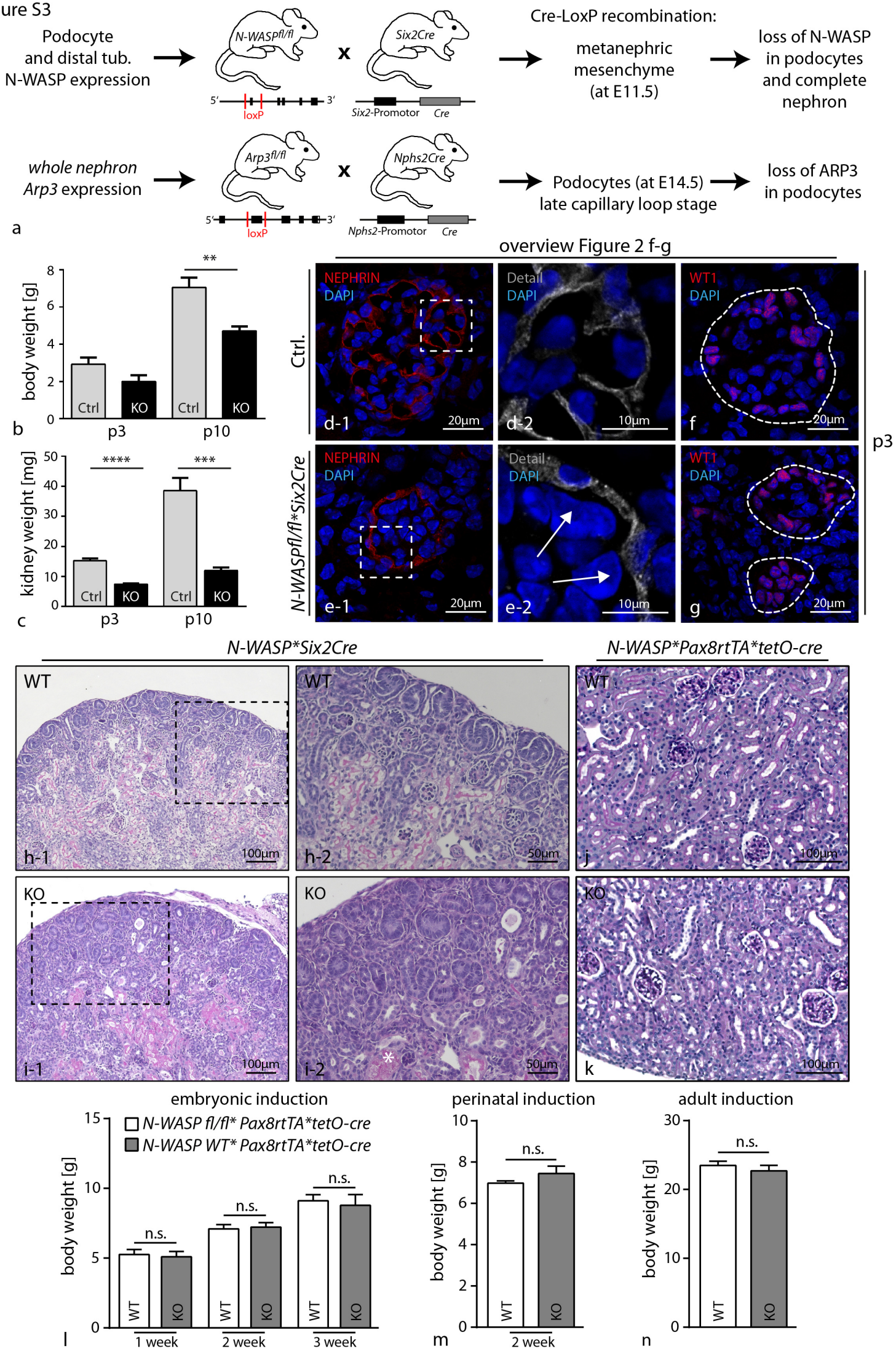
Podocyte and distal tub. N-WASP expression
N-WASPfl/fl
Six2Cre
Six2-Promotor
Cre
loxP
Cre-LoxP recombination:
metanephric mesenchyme (at E11.5)
loss of N-WASP in podocytes and complete nephron
whole nephron Arp3 expression
Arp3fl/fl
Nphs2Cre
Nphs2-Promotor
Podocytes (at E14.5) late capillary loop stage
loss of ARP3 in podocytes
a
overview Figure 2 f-g
body weight [g]
Ctrl
KO
p3
p10
b
kidney weight [mg]
c
NEPHRIN
DAPI
Detail
WT1
Ctrl.
N-WASPfl/fl*Six2Cre
d-1
d-2
e-1
e-2
f
g
20µm
10µm
p3
N-WASP*Six2Cre
N-WASP*Pax8rtTA*tetO-cre
WT
KO
h-1
h-2
i-1
i-2
j
k
100µm
50µm
embryonic induction
perinatal induction
adult induction
N-WASP fl/fl* Pax8rtTA*tetO-cre
N-WASP WT* Pax8rtTA*tetO-cre
n.s.
1 week
2 week
3 week
l
m
n

Figure S4

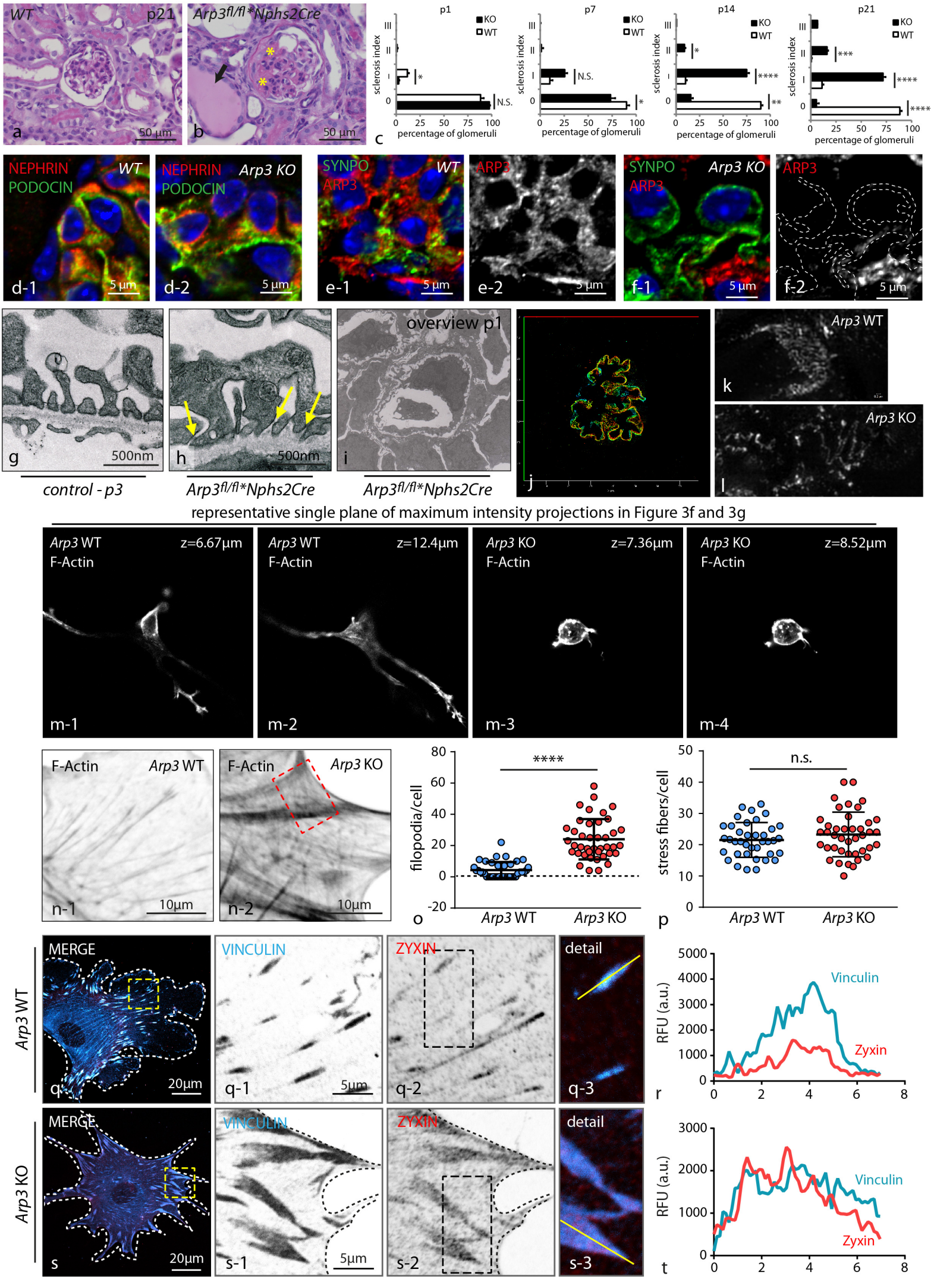
WT
p21
a
50 µm
Arp3fl/fl*Nphs2Cre
b
50 µm
c
p1
p7
p14
p21
KO
WT
sclerosis index
III
II
I
0
N.S.
*
**
***
****
0 25 50 75 100
percentage of glomeruli
NEPHRIN
PODOCIN
WT
d-1
5 µm
Arp3 KO
d-2
SYNPO
ARP3
e-1
e-2
f-1
f-2
g
500nm
h
i
overview p1
j
Arp3 WT
k
Arp3 KO
l
control - p3
Arp3fl/fl*Nphs2Cre
representative single plane of maximum intensity projections in Figure 3f and 3g
F-Actin
z=6.67µm
m-1
z=12.4µm
m-2
z=7.36µm
m-3
z=8.52µm
m-4
n-1
10µm
n-2
o
filopodia/cell
80
60
40
20
0
-20
****
p
stress fibers/cell
50
40
30
20
10
0
n.s.
MERGE
VINCULIN
ZYXIN
detail
q
20µm
q-1
5µm
q-2
q-3
r
RFU (a.u.)
5000
4000
3000
2000
1000
0
Vinculin
Zyxin
s
s-1
s-2
s-3
t

Figure S5

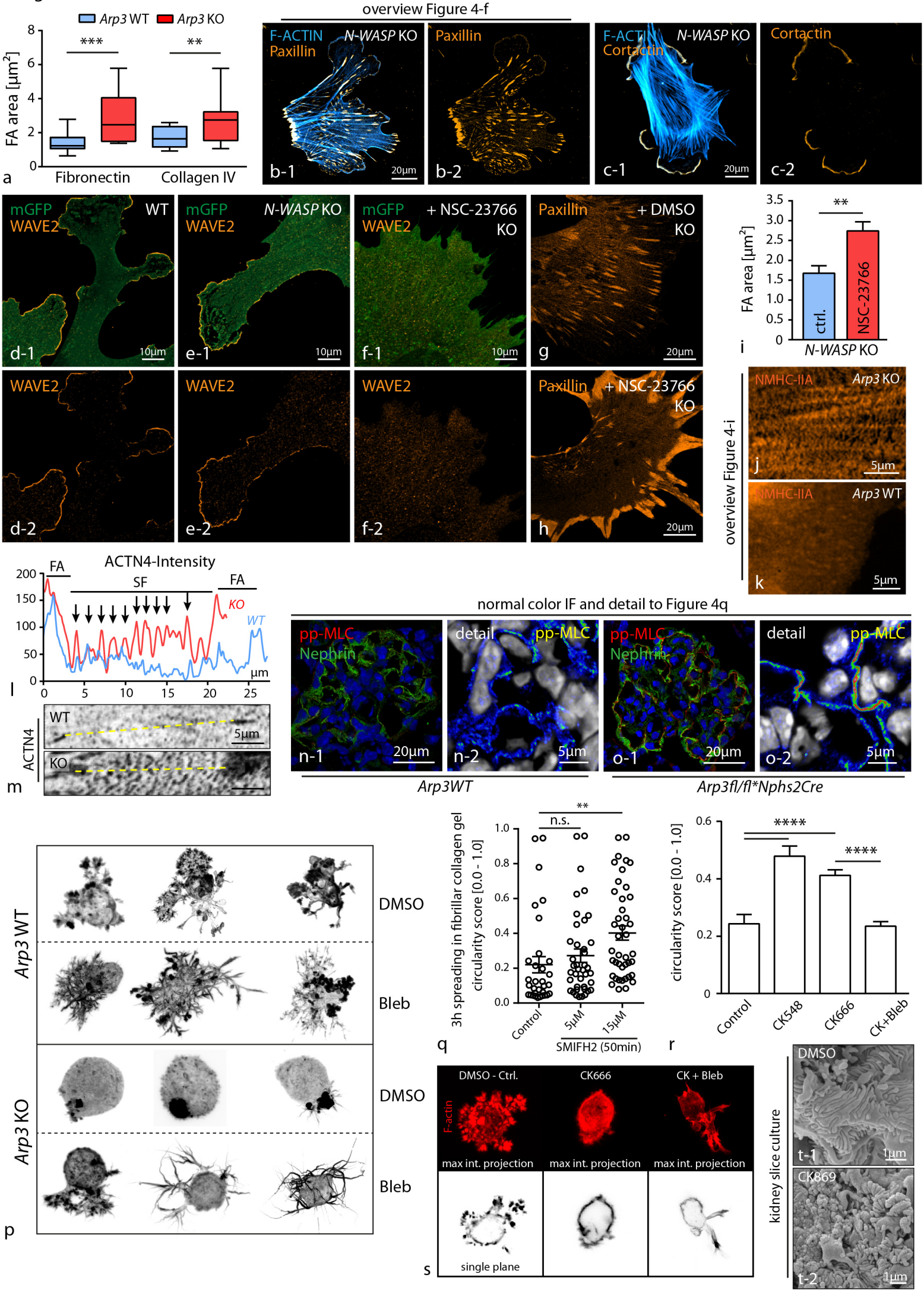
Arp3 WT
Arp3 KO
FA area [µm²]
***
**
Fibronectin
Collagen IV
a
overview Figure 4-f
F-ACTIN
Paxillin
N-WASP KO
b-1
20µm
b-2
Cortactin
c-1
c-2
mGFP
WAVE2
WT
d-1
10µm
e-1
+ NSC-23766
KO
f-1
+ DMSO
g
20µm
d-2
e-2
f-2
h
i
ctrl.
NSC-23766
N-WASP KO
overview Figure 4-i
NMHC-IIA
Arp3 KO
j
5µm
Arp3 WT
k
ACTN4-Intensity
FA
SF
KO
WT
µm
l
ACTN4
m
normal color IF and detail to Figure 4q
pp-MLC
Nephrin
detail
n-1
n-2
o-1
o-2
Arp3WT
Arp3fl/fl*Nphs2Cre
Arp3 WT
Arp3 KO
DMSO
Bleb
p
3h spreading in fibrillar collagen gel
circularity score [0.0 - 1.0]
n.s.
Control
5µM
15µM
SMIFH2 (50min)
q
****
CK548
CK666
CK+Bleb
r
DMSO - Ctrl.
CK666
CK + Bleb
F-actin
max int. projection
single plane
s
kidney slice culture
t-1
1µm
CK869
t-2

Figure S6

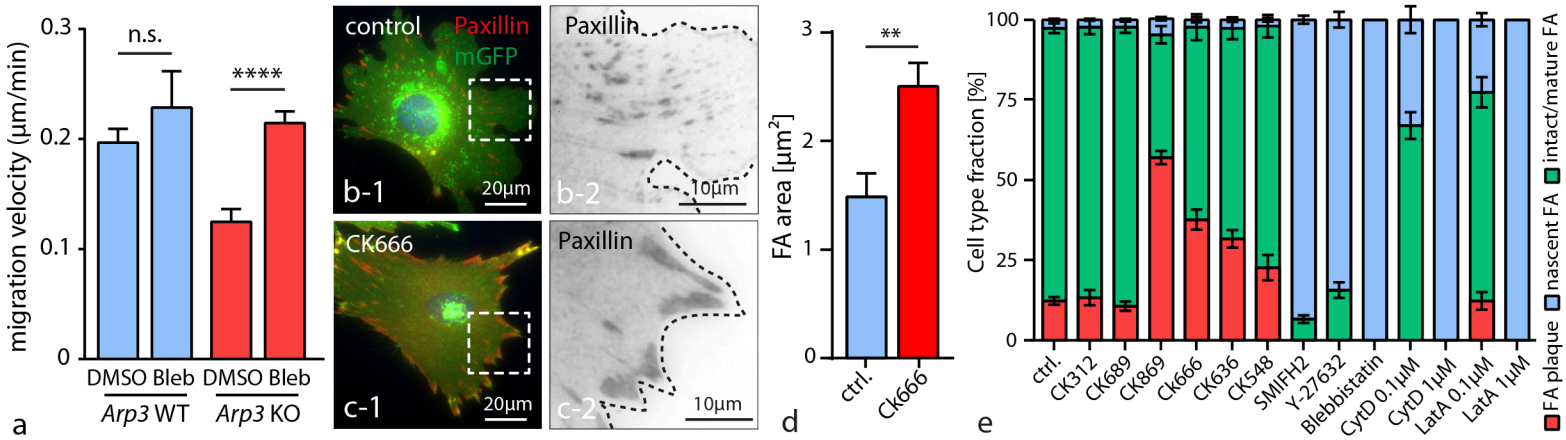
migration velocity (µm/min)
n.s.
****
DMSO Bleb DMSO Bleb
Arp3 WT Arp3 KO
a
control Paxillin mGFP
b-1
20µm
Paxillin
b-2
10µm
CK666
c-1
20µm
Paxillin
c-2
10µm
FA area [µm²]
**
ctrl. Ck666
d
Cell type fraction [%]
ctrl. CK312 CK689 CK869 Ck666 CK636 CK548 SMIFH2 Y-27632 Blebbistatin CytD 0.1µM CytD 1µM LatA 0.1µM LatA 1µM
FA plaque nascent FA intact/mature FA
e

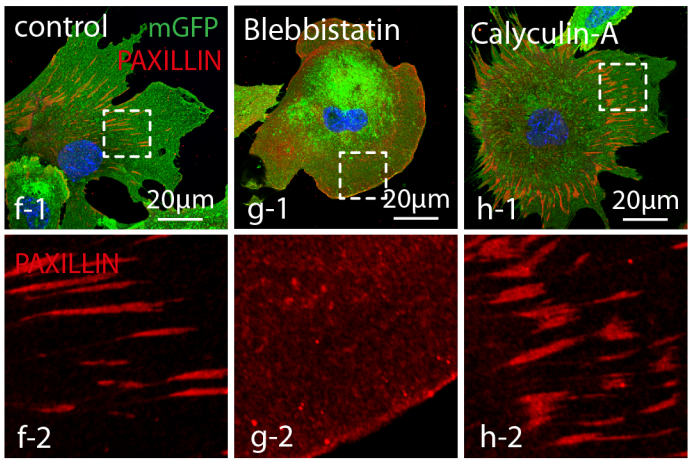
control mGFP PAXILLIN
f-1
20µm
Blebbistatin
g-1
20µm
Calyculin-A
h-1
20µm
PAXILLIN
f-2
g-2
h-2

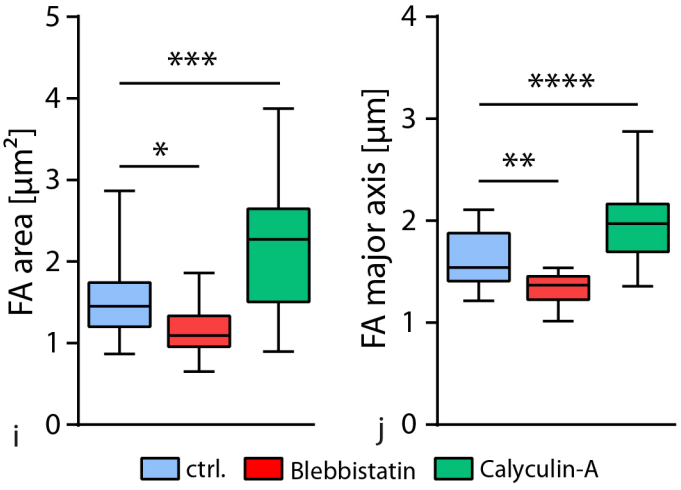
FA area [µm²]
***
*
i
FA major axis [µm]
****
**
j
ctrl. Blebbistatin Calyculin-A

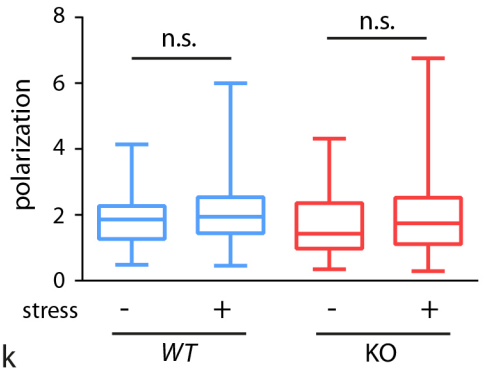
polarization
n.s.
n.s.
stress - + - +
WT KO
k

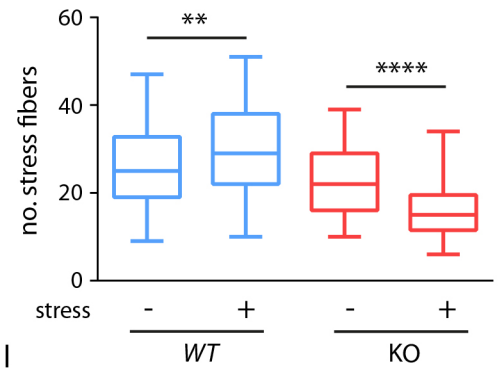
no. stress fibers
**
****
stress - + - +
WT KO
l

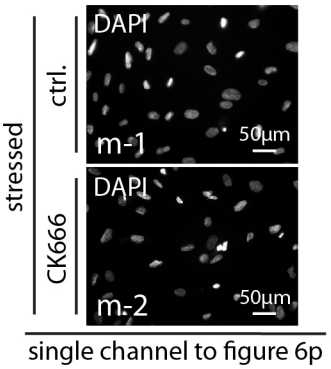
stressed
ctrl.
CK666
DAPI
m-1
50µm
DAPI
m-2
50µm
single channel to figure 6p

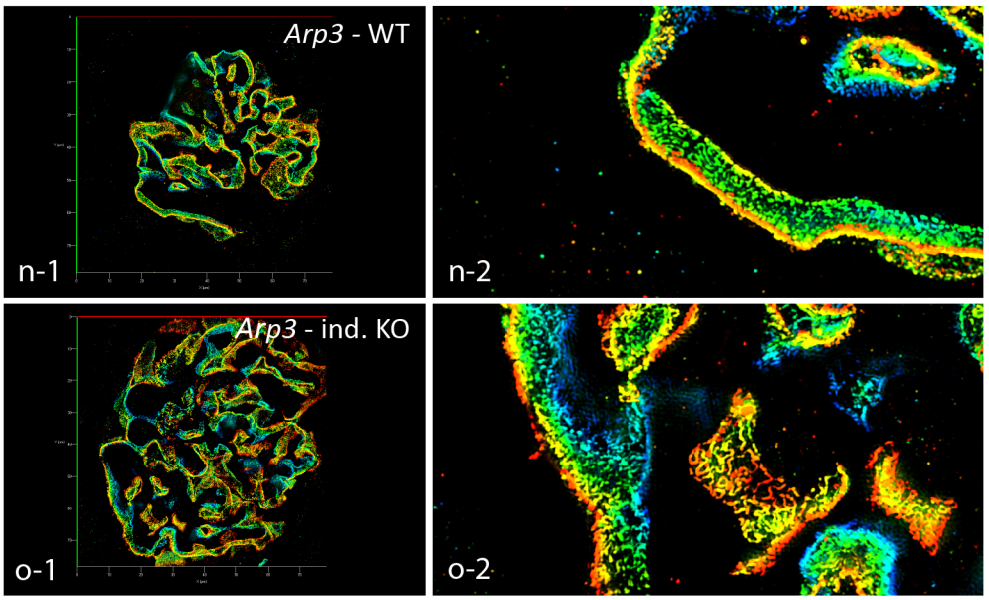
Arp3 - WT
n-1
n-2
Arp3 - ind. KO
o-1
o-2

Figure S7

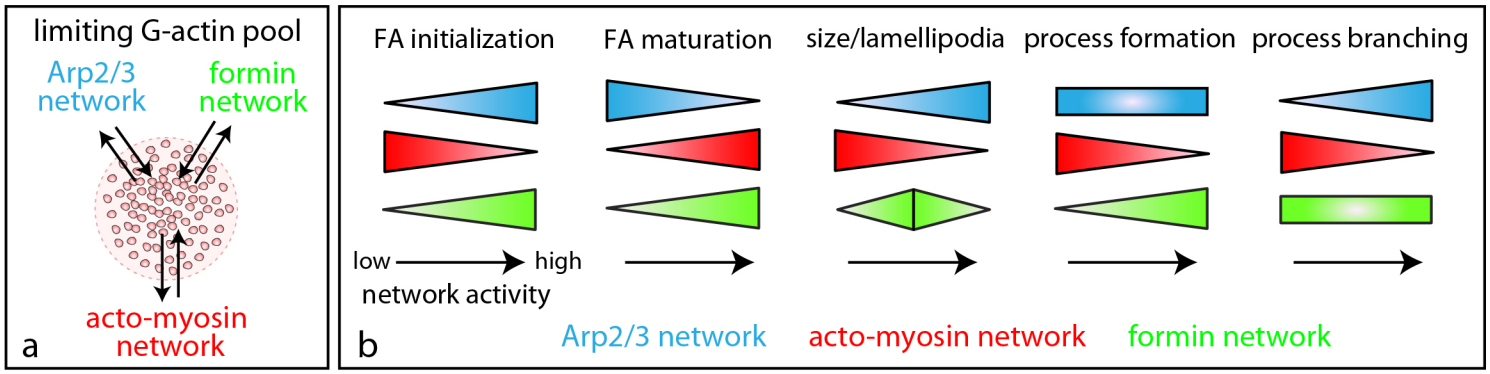

Figure 1
WB: ACTR3

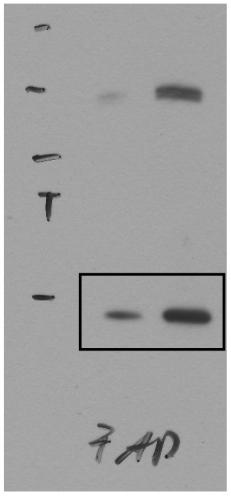

Figure 1
WB: PXN

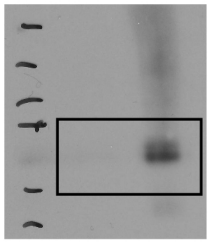

Figure 1
WB: PDH

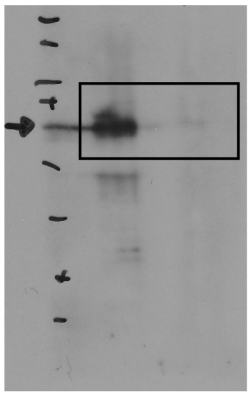

Figure 2
WB: ACTR3

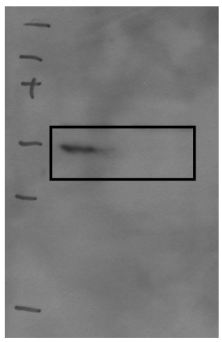

Figure 2
WB: TUBA

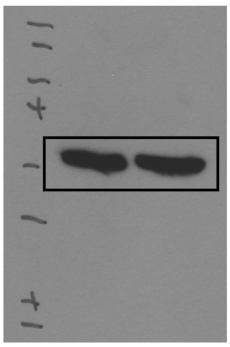

Figure 7
WB: WT1

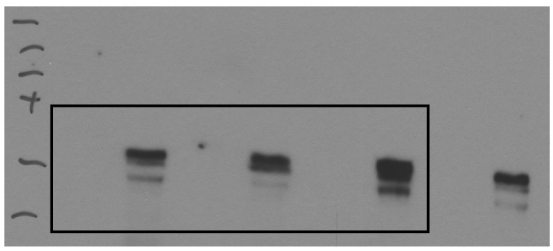

Figure S3
WB: ITGB1

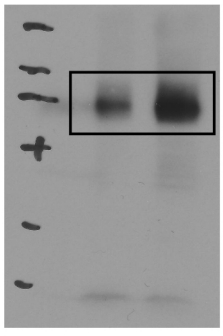

Figure S3
WB: ACTN4